Modification and Control of Topological Insulator Surface States Using Surface Disorder

Vincent Sacksteder*
School of Physical and Mathematical Sciences, Nanyang Technological University, 637371 Singapore, Singapore

Tomi Ohtsuki and Koji Kobayashi
Department of Physics, Sophia University, Tokyo 102-8554, Japan

(Received 14 December 2014; revised manuscript received 27 February 2015; published 11 June 2015)

We numerically demonstrate a practical means of systematically controlling topological transport on the surface of a three-dimensional topological insulator, by introducing strong disorder in a layer of depth d extending inward from the surface of the topological insulator. The dependence on d of the density of states, conductance, scattering time, scattering length, diffusion constant, and mean Fermi velocity are investigated. The proposed control via disorder depth d requires that the disorder strength be near the large value which is necessary to drive the topological insulator into the nontopological phase. If d is patterned using masks, gates, ion implantation, etc., then integrated circuits may be fabricated. This technique will be useful for experiments and for device engineering.

DOI: 10.1103/PhysRevApplied.3.064006

I. INTRODUCTION

Recently, a new kind of material has been predicted and measured: topological insulators, which do not permit current to flow through their interior but do allow metallic conduction along their surfaces [1–5]. The conducting states residing on the topological insulator (TI) surface are protected topologically, meaning that they are safeguarded by the bulk's insulating property from local perturbations as long as a mobility gap is maintained between the bulk bands. Consequently, the surface states are only weakly sensitive to the fine details of the bulk Hamiltonian, such as lattice structure, details of atomic bonding, or interactions. They are, however, vulnerable to any conduction through the bulk at energies lying in the bulk band gap and, therefore, demand a very high-purity bulk. Any engineering of TI devices for either practical or scientific applications will likely use a very pure and unaltered TI bulk and utilize only the TI's surface.

There are several compelling motivations for using TI surfaces instead of conventional materials to carry current. Power dissipation may be reduced by the TI's robustness against disorder. TIs also lock spin to momentum, which will be useful for creating spin-polarized currents and for conducting spin over long distances. They may also host exotic states that could be used for quantum computing, such as Majorana fermions or strongly interacting topological phases [6–8]. However, these applications all suffer from the topological state's resilience against the mechanisms usually employed to direct or switch off electronic conduction, such as gating and etching. TI surface states are difficult to control.

In this article, we propose a way of engineering TI device properties to match engineering requirements. Our main contribution is the observation that introducing disorder *only near the TI's surface*, in a region beginning on the TI surface and extending inward to a depth d, is a practical way of controlling the surface states. As the electron moves across the disordered surface of the TI, from time to time it becomes almost trapped at a particular site and dwells there for a while before continuing its journey. This trapping is unable to destroy or localize the in-gap surface state, but it does cause a localized increase in the surface state's probability density, and our numerical results show a corresponding increase in the in-gap density of states ρ. Moreover, the increased dwell times at individual sites cause, on average, a decrease in the Fermi velocity v_F. The altered density of states and Fermi velocity change also the scattering time τ, diffusion constant $D = v_F^2\tau/2$, and coupling constant $\alpha = e^2/\epsilon\hbar v_F$ controlling interactions.

The impact of surface disorder on a topologically protected state is ordinarily limited by the state's tendency to shift into the clean bulk to avoid disorder. However, we can trap the topological state in the disordered region by tuning the disorder strength W near the critical value W_c which causes the disordered TI to transit from the topological phase to the nontopological phase.

Our main point is to demonstrate that when the topological state is trapped in the disordered region, it is strongly sensitive to the disorder depth d. This is a unique control parameter, which, if patterned on a TI surface, can create areas with slower conduction and increased density of states, introduce control points that are sensitive to

*vincent@sacksteder.com

gating voltages, and direct conduction along particular channels.

We emphasize that there are several practical and achievable techniques for producing patterned surface disorder. Already, many experiments have studied the effects on TI surfaces of disorder induced by atmosphere, by deliberate introduction of adsorbed molecules and dopants, and even by mechanical surface abrasion [9–18]. Numerous experiments have also demonstrated that capping can effectively protect a TI surface, so masking and etching techniques are promising, as is ion implantation [19].

Ion implantation, in particular, gives precise control of impurity concentration and depth and allows control of the Fermi level by mixing ions. This technique has been developed extensively for applications to semiconductors, but its application to TIs is at an exploratory stage. The related technique of ion milling, useful for controlling sample thickness and for polishing the surface, was first applied to TIs in 2010, and is now in widespread use [20]. Ion implantation was first applied to TIs in studies of the spin response to a magnetic field [21,22], and more recently has been used to dope the Fermi level [23] and to add disorder to the TI surface [24].

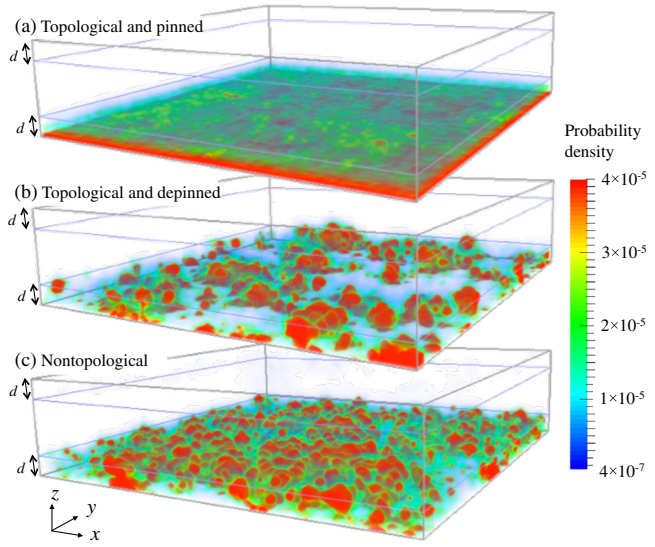

FIG. 1. The three types of transport illustrated in a disordered surface layer of depth $d = 5$. Panel (a) shows the probability density $|\psi|^2$ at small disorder $W = 4.5$; the topological state is pinned to the sample's bottom surface. Panel (b) shows a topological state at $W = 7.5$, near W_c. It is fully depinned from the bottom surface but, nonetheless, supports topologically protected conduction. Panel (c) shows strong disorder $W = 9.0$, where the disordered region is no longer topological and hosts the bulk states seen here. A topological state at the disorder boundary coexists with these bulk states, and both contribute to the conductivity. The sample dimensions are $l \times w \times h = 80 \times 80 \times 20$, with periodic boundary conditions in the x and y directions, and $E_F \approx 0$.

The surface-state control which is proposed here is obtained only at the critical disorder $W \approx W_c$, which is generally quite large, roughly the same as the bulk band width E_B, but can be reduced to much smaller values by tuning the Fermi level [25,26]. At small disorder $W \ll W_c$ the topological state is pinned at the outer boundary of the disordered region, as seen in Fig. 1(a). Its conduction is, therefore, insensitive to the region's depth. In the opposite case of large disorder $W \gg W_c$, the disordered region fills with nontopological states deriving from the bulk band [Fig. 1(c)] [27–30] which contribute to conduction, and the conductance and the density of states both depend on d. Only near $W \approx W_c$ does the topological state depin from the TI's outer surface and stretch inward to the interface with the clean bulk [Fig. 1(b)], producing conduction which is both topological and sensitive to the disorder depth d.

In Sec. II, we analyze these three types of transport and determine in each case how the transport parameters scale with the disorder depth d. Next, Sec. III presents our numerical model and confirms numerically the existence of the depinned topological state whose transport can be controlled by disorder depth. We conclude with Sec. IV, which discusses how to pattern topological conduction to meet device requirements.

II. SCALING ANALYSIS OF DISORDERED TRANSPORT

Depending on the disorder strength, three different types of conducting states may be obtained. These states have clear signatures in the dependence of the conductance G and the 2D density of states ρ_{2D} on disorder depth d, which we show in Table I and will exhibit in our numerical results. The *pinned topological state* at $W \ll W_c$ is not sensitive to d. At the other extreme $W \gg W_c$, *nontopological states* in the disordered region are important. The scattering length l of these strongly disordered states is comparable to the lattice spacing and much smaller than the disorder depth, so these states undergo true 3D diffusive transport, with G and ρ_{2D} both linear in d.

In contrast, the *depinned topological state* at $W \approx W_c$ can be identified clearly by the signature of a d-linear 2D DOS ρ_{2D} combined with a constant conductance G. The linear ρ_{2D} is caused by the state depinning from the

TABLE I. The transport parameters' scaling with disorder depth d. G is the conductance, ρ_{2D} is the density of states, v_F is the mean Fermi velocity, τ is the scattering time, l is the scattering length, D is the diffusion constant, and α is the dimensionless coupling constant governing interactions.

Conducting state	G	ρ_{2D}	v_F	τ	$l = v_F\tau$	D	α
Topological and pinned	1	1	1	1	1	1	1
Topological and depinned	1	d	$1/d$	d	1	$1/d$	d
Nontopological	d	d	1	1	1	1	1

TI surface, while the constant G controverts nontopological conduction, which would exhibit 3D diffusion and a linear conductance.

This signature is unambiguous. The linear DOS cannot be attributed to any nontopological surface or bulk states distinct from the depinned topological state, because all in-gap states are located in the disordered region, which near W_c delocalizes and hosts only extended states like that seen in Fig. 1(b). In the parallel case of 2D TIs with edge disorder, very few in-gap states are localized, and the conductance remains quantized [29,31,32]. In both 2D and 3D at $W \approx W_c$ all states mix and participate in the topological conduction.

The depinned state is very remarkable for being simultaneously robustly conducting and extremely disordered. This is seen clearly in Fig. 1, where we calculate the states' inverse participation ratios (IPRs), a measure of their volumes defined by $\sum_i [\sum_{\alpha=1}^{4} |\psi(i,\alpha)|^2]^2$ with $\psi(i,\alpha)$ the αth component of the wave function on the site i. These eigenfunctions are obtained by diagonalizing the Hamiltonian using the sparse matrix diagonalization subroutine FEAST built with the Intel FORTRAN Math Kernel Library. The system size is $80 \times 80 \times 20$, and periodic boundary conditions are imposed in the x and y directions, while the open boundary condition is imposed in the z direction. The IPR of the wave function of the depinned state [Fig. 1(b)] is 2.09×10^{-3}, an order of magnitude larger than those of the pinned and bulk states [Figs. 1(a) and 1(c)], which are 1.25×10^{-4} and 1.73×10^{-4}, respectively. In nontopological systems, this type of volume reduction will be accompanied by Anderson localization, i.e., the state's extent along the x and y axes parallel to the surface will be much smaller than the sample size. Here, topology ensures that the depinned state remains conducting and extended across the entire sample.

The depinned state is topologically guaranteed to conduct over large distances and, therefore, must have a long-wavelength limit where the average parameters of 2D surface transport are well defined, including the 2D density of states ρ_{2D}, average Fermi velocity v_F, etc. [29]. We will show that these quantities are strongly dependent on d, beginning with the Fermi velocity $v_F = dE/dk$, the eigenvalue's derivative with respect to k. Its scaling can be determined from the fact that the depinned topological state is not localized. Therefore, the eigenvalues within the gap repel each other according to Wigner-Dyson level repulsion, and the energy scale dE in $v_F = dE/dk$ is set by the level spacing ΔE [29]. The depinned state extends inward to depth d, so its 2D DOS ρ_{2D} is proportional to d, and ΔE scales with $1/d$. Since in strongly disordered samples the momentum scale dk in v_F is controlled by the inverse of the lattice spacing a and is not sensitive to d, we obtain $v_F \propto 1/d$.

Next, we note that at $W \approx W_c$ the scattering length l is close to the lattice spacing and independent of d. Since $l = v_F\tau$, the scattering time grows linearly with d, inversely to ΔE. We report these scaling relations, along with $D = v_F^2\tau/2$ and the dimensionless coupling constant $\alpha = e^2/(\epsilon\hbar v_F)$ which controls interaction effects, in Table I [33]. Table I's results for the depinned state can be determined directly from dimensional analysis by finding each quantity's scaling with either the scattering time $\tau \propto d$ or its inverse, the energy $\propto 1/d$. In summary, v_F, τ, D, and α are all very sensitive to the disorder depth d, while G and l are not.

III. NUMERICAL RESULTS

We turn to calculations of the effect of disorder depth d on ρ and G, which will confirm numerically the existence of a depinned topological state with the scaling listed in Table I. The topological surface conduction which interests us is independent of any microscopic details of the Hamiltonian. Therefore, we study a computationally efficient minimal tight binding model of a strong $\mathbb{Z}_2$ TI implemented on a cubic lattice. We leave the TI bulk pure, since the main effects of bulk disorder can be duplicated by narrowing the bulk band gap and increasing the penetration depth in a pure TI [25,26,34–36]. We also omit the effects of bulk defects, which are known to dope the Fermi level toward the conduction band or valence band depending on the defect type and at sufficient concentrations also cause a conducting impurity band to be formed inside the bulk band gap [37]. We will return to doping in Sec. IV. With four orbitals per site, the model's momentum representation is

$$H = \sum_{i=1}^{3} \left[\left(\imath \frac{t}{2} \alpha_i - \frac{1}{2}\beta \right) e^{-\imath k_i a} + \text{H.c.} \right] + (m+3)\beta, \quad (1)$$

$\alpha_i = \sigma_x \otimes \sigma_i$ and $\beta = \sigma_z \otimes 1$ are gamma matrices in the Dirac representation, $t = 2$ is the hopping strength, $m = -1$ is the mass parameter, and $a = 1$ is the lattice spacing [36,38–40]. This noninteracting model exhibits a bulk band gap in the interval $E_F = [-|m|, |m|]$ and a single Dirac cone in the bulk gap. To this model we add uncorrelated white-noise disorder $u(x)$ chosen randomly from the interval $[-W/2, W/2]$, where W is the disorder strength. In the 3D limit, this model's topological phase transition occurs at $W_c \approx 7.5$ when the Fermi energy is at the Dirac point [36,41]. The disorder is added only on the d layers nearest the TI sample's upper boundary and also the d layers nearest the lower boundary, as shown in Fig. 2. Each of these layers has the same disorder strength, and the interior is left clean, so the disorder's spatial profile is a step function.

We will present numerical results about the global density of states $\rho(E)$ and the conductance $G(E)$. The density of states is defined as $\rho(E) = \text{Tr}[\delta(E - H)]$, where

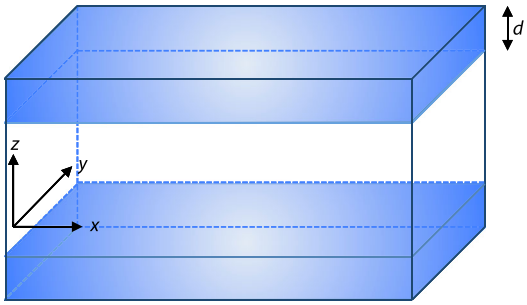

FIG. 2. Schematic of the sample geometry. The shaded region is disordered. In the calculation of the density of states, periodic boundary conditions (PBC's) are imposed in the x and y directions. In the conductance calculation, pbc's are imposed in the y direction and current flows in the x direction. In both cases, fixed boundary conditions are imposed in the z direction.

δ is the matrix version of the Dirac δ-function. We calculate $\rho(E)$ in large $400 \times 400 \times 20$ slabs, with periodic boundary conditions in the slab plane, using the highly scalable kernel polynomial method [42]. $\mathrm{Tr}[\delta(E-H)]$ is approximated with an expansion in its Chebyshev moments, the resulting sum over moments is truncated at some maximum number of moments, and this truncation is smoothed using the Jackson kernel. We verify convergence by systematically recalculating our results with different numbers of moments going as high as 10 000 moments. We find that the density of states is self-averaging so that ten samples are sufficient to obtain high-accuracy results.

For the conductance, we use the Landauer formula $G = G_0 \mathrm{Tr}(\boldsymbol{t}^\dagger \boldsymbol{t})$, where $G_0 = e^2/h$ is the conductance quantum and we average over 100 statistical realizations. $\boldsymbol{t}$ is the TI's transmission matrix, which we compute using the transfer-matrix method [43–45]. We calculate the conductance at zero temperature so only states at the Fermi level E_F contribute, in contrast to finite temperatures where the Fermi level is smeared across a range of order $k_B T$. Since the critical disorder strength W_c depends on the Fermi level, at nonzero temperature the conductance will have contributions not only from the topological depinned state but also from the topological pinned state and the nontopological state. The size of these contributions and also of the conductance from thermally activated bulk carriers can be controlled by reducing the temperature.

We minimize the leads' effects by using metallic leads. Each TI site adjacent to the leads is connected to a perfectly conducting 1D wire, similar to network models. We use a slab of height $h = 20$, length $l = 40$ between the two leads, and width $w = 40$ with periodic boundary conditions along this transverse axis. The scattering length is less than 40 for all disorder strengths greater than $W > 2$, so finite-size effects from the sample width and length are small [30]. Moreover, because we study disordered boundaries whose maximum depth is $d = 5$ layers, the two disordered boundary layers are always separated by at least ten layers of pure nondisordered bulk. Changing the clean bulk's depth from 10 to 15 while keeping $d = 5$ fixed confirms that the conductance is unchanged when the disorder in the boundary is not too large ($W = 3, 6$ at $E_F = 0, 0.25$), but at larger disorder the conductance increases. Since the clean bulk's depth is equal to $h - 2d = 20 - 2d$, and our numerical results keep $h = 20$ fixed, our results on the conductance's depth dependence underestimate the behavior of a thick slab. This does not affect our qualitative conclusions.

In Fig. 3 we focus our attention on the normalized density of states in the bulk gap $E_F = [-1, 1]$, where the topological surface states are found. The smallest-disorder curves are linear in E_F, i.e., $\rho \propto |E_F|$, which is a hallmark of 2D Dirac fermions. As seen in the inset, the slope grows with increasing disorder, because disorder causes a decrease in the Fermi velocity $v_F = dE/dk$. At larger disorder $W \geq 3$, the DOS departs from the linear Dirac form in two intervals near $E_F = \pm 1$, and by $W \geq 6$ these intervals expand to fill the whole band gap. In these intervals, the topological state consecutively becomes strongly disordered, depins, and then is joined by nontopological states in the disordered region [28,29]. In particular, depinned states occur at two critical energies $E_c(W)$, which, in the disorder-free $W = 0$ case, lie at the band edges $E_c = \pm 1$ but move inward toward the Dirac point as the disorder grows stronger. At $W = W_c$, the critical energies meet at the Dirac point $E_F = 0$, and at larger $W > W_c$ the disordered region no longer hosts topological states. The detailed values of E_c, W_c are material dependent, but the qualitative behavior described here is generic to every topological insulator.

Figure 4 shows signatures of the three types of conducting states in the dependence on depth d of the DOS ρ

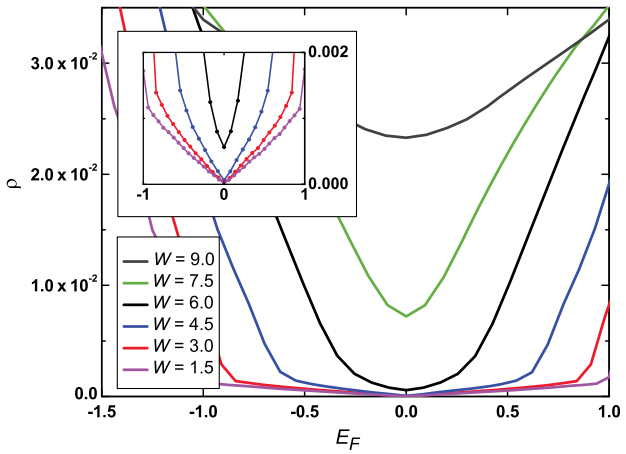

FIG. 3. The normalized density of states inside the bulk gap evolving from small disorder $W = 1.5$ to large disorder $W = 9$. The disorder depth is $d = 5$. The inset shows that at small disorder the DOS is linear in E_F, which signals that here the Dirac cone is intact.

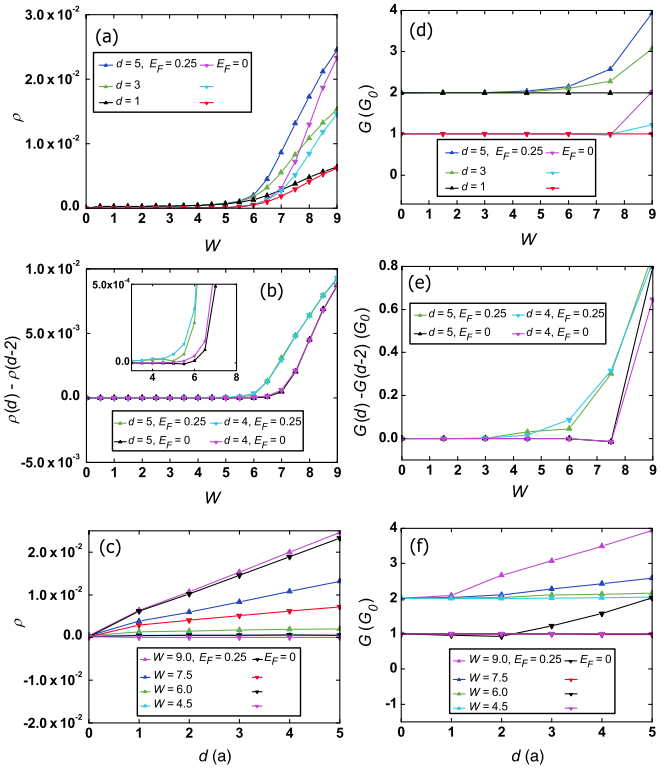

FIG. 4. Transport signatures in the DOS ρ (left panels) and conductance G (right panels) at two values of the Fermi level $E_F = 0, 0.25$. We shift the $E_F = 0$ conductance downward by G_0 for clarity. The pinned topological state is indicated when ρ is independent of the disorder depth d. Nontopological states are indicated when G is linear in d. The depinned topological state shows a constant G and linear ρ. Panels (a) and (d) show the dependence on W. Panels (b) and (e) show the change in ρ and G caused by adding two disorder layers. Panels (c) and (f) demonstrate linearity in d.

(left panels) and the conductance G (right panels). Figures 4(a) and 4(d) show that at small disorder, both ρ and G are independent of d, as expected from the $W \ll W_c$ pinned topological state. At stronger disorder, both quantities become sensitive to d, as expected of $W \gg W_c$ nontopological states in the strongly disordered region. Figures 4(c) and 4(f) demonstrate that the d dependence is always roughly linear.

Figures 4(b) and 4(e) allow us to pinpoint the transition from no d dependence to linear dependence, by plotting the magnitude of the change when d is changed from 2 to 4, and from 3 to 5. Figure 4(b) shows that at $E_F = 0, 0.25$, the DOS becomes dependent on d starting at $W \approx 6.5, 5.5$, and the d dependence becomes large around $W \approx 7.0, 6.5$. This transition signals depinning from the TI surface shown in Fig. 1(b). Figure 4(e) shows that G remains constant in d at $W = 6$ for $E_F = 0$ and nearly constant also at $W = 7.5, E_F = 0$. In this region, we have constant G and linear ρ, which is the signature of the depinned topological state.

In summary, we confirm numerically that the depinned state's conduction obeys the depth dependence in Table I, which is based on the fact that this state is both very strongly disordered and robustly conducting. Consequently, its scattering time τ scales linearly with the disorder depth d, and its scattering length is independent of d. This determines the depth dependence of all other conduction parameters.

IV. APPLICATIONS

Using this effect, a topological state's conduction can be engineered and patterned to meet device requirements by introducing a layer of strong $W \approx W_c$ surface disorder and patterning the layer's depth d. d must substantially exceed the bulk penetration depth λ, which is typically 2–3 nm in the Bi_2Se_3 family of TIs [46]. It is necessary that the disorder's spatial distribution has a step function profile; the disorder strength should be constant from the surface up to depth d and then drop to zero. Ion implantation produces a Gaussian depth distribution around a mean depth controlled by the beam energy; a step function distribution may be approximated by applying the beam twice at two different beam energies.

Increasing the density of states of the in-gap surface states will make them less sensitive to bulk defects, which are known to cause bulk conduction by introducing carriers. Depending on the defect type, the defects shift the Fermi level toward either the valence band or the conduction band [47,48]. When disorder is used to increase the surface density of states, the Fermi level will be less sensitive to bulk defects and shift further into the gap, increasing the TI quality. In patterned devices, points with increased disorder depth d and density of states ρ will respond more strongly to external static or ac voltages. Interaction with light also will be increased if the light's penetration depth exceeds λ [49]. Moreover, the state's self-interaction will be increased, which favors transitions to strongly interacting topological phases [7,8].

Engineered lines of increased d on a TI surface can be used to direct the topological current's flow across the surface and to divide current flow and later reunite it, similar to integrated circuits in conventional semiconductor devices. These channels can be controlled by using external gates to locally shift the Fermi level. Because the critical disorder W_c is sensitive to the Fermi level E_F, if the Fermi level is either too large or too small then the topological state will reroute to the boundary of the disordered region and will lose its depth dependence. Therefore, external gates can control the density of states at specific points on the TI surface, regulating the current flow through channels, or switching current from one channel to another. In summary, the topological current can be focused, directed along particular channels, and switched, supplying all of the components necessary for realizing topological integrated circuits.

We conclude by discussing a specific device, a spectral analyzer of incoming transient pulses. Its crucial component is a region where the disorder depth d grows continuously. A topological state diffusing through this region will experience a spatially nonuniform scattering time τ. Its diffusion is similar to Brownian motion of classical particles in the presence of a temperature gradient, since the time between Brownian steps varies inversely with the temperature. As is well known from the celebrated Ludwig-Soret thermodiffusion effect, the diffusing state will experience an effective force deflecting it along the gradient of τ and d [50–52]. The deflection is greatest when the topological state's energy E is at the critical value E_c associated with depinning, so the spectral analyzer will spatially resolve incoming pulses according to their component energies.

ACKNOWLEDGMENTS

We thank Quansheng Wu, Liang Du, Alex Petrovic, and Ken-Ichiro Imura for very useful discussion and collaboration, and Ivan Shelykh for his support. This work was supported by JSPS KAKENHI Grants No. 15H03700 and No. 24000013. Part of the numerical calculation has been performed on the Supercomputer System B of ISSP, The University of Tokyo.

[1] C. L. Kane and E. J. Mele, Quantum Spin Hall Effect in Graphene, Phys. Rev. Lett. **95**, 226801 (2005).

[2] Haijun Zhang, Chao-Xing Liu, Xiao-Liang Qi, Xi Dai, Zhong Fang, and Shou-Cheng Zhang, Topological insulators in Bi_2Se_3, Bi_2Te_3 and Sb_2Te_3 with a single Dirac cone on the surface, Nat. Phys. **5**, 438 (2009).

[3] M. Z. Hasan and C. L. Kane, Colloquium: Topological insulators, Rev. Mod. Phys. **82**, 3045 (2010).

[4] Yong-qing Li, Ke-hui Wu, Jun-ren Shi, and Xin-cheng Xie, Electron transport properties of three-dimensional topological insulators, Front. Phys. **7**, 165 (2012).

[5] Dimitrie Culcer, Transport in three-dimensional topological insulators: Theory and experiment, Physica (Amsterdam) **44E**, 860 (2012).

[6] Liang Fu and C. L. Kane, Superconducting Proximity Effect and Majorana Fermions at the Surface of a Topological Insulator, Phys. Rev. Lett. **100**, 096407 (2008).

[7] B. Swingle, M. Barkeshli, J. McGreevy, and T. Senthil, Correlated topological insulators and the fractional magnetoelectric effect, Phys. Rev. B **83**, 195139 (2011).

[8] Joseph Maciejko, Xiao-Liang Qi, Andreas Karch, and Shou-Cheng Zhang, Fractional Topological Insulators in Three Dimensions, Phys. Rev. Lett. **105**, 246809 (2010).

[9] David Hsieh, Y. Xia, Dong Qian, L. Wray, J. H. Dil, F. Meier, J. Osterwalder, L. Patthey, J. G. Checkelsky, N. P. Ong *et al.*, A tunable topological insulator in the spin helical Dirac transport regime, Nature **460**, 1101 (2009).

[10] Marco Bianchi, Dandan Guan, Shining Bao, Jianli Mi, Bo Brummerstedt Iversen, Philip D. C. King, and Philip Hofmann, Coexistence of the topological state and a two-dimensional electron gas on the surface of Bi_2Se_3, Nat. Commun. **1**, 128 (2010).

[11] James G. Analytis, Jiun-Haw Chu, Yulin Chen, Felipe Corredor, Ross D. McDonald, Z. X. Shen, and Ian R. Fisher, Bulk Fermi surface coexistence with Dirac surface state in Bi_2Se_3: A comparison of photoemission and Shubnikov–de Haas measurements, Phys. Rev. B **81**, 205407 (2010).

[12] Han-Jin Noh, Jinwon Jeong, En-Jin Cho, Han-Koo Lee, and Hyeong-Do Kim, Persistence of surface states despite impurities in the surface of topological insulators, Europhys. Lett. **96**, 47002 (2011).

[13] Desheng Kong, Judy J. Cha, Keji Lai, Hailin Peng, James G. Analytis, Stefan Meister, Yulin Chen, Hai-Jun Zhang, Ian R. Fisher, Zhi-Xun Shen *et al.*, Rapid surface oxidation as a source of surface degradation factor for Bi_2Se_3, ACS Nano **5**, 4698 (2011).

[14] Oleg Evgen'evich Tereshchenko, K. A. Kokh, V. V. Atuchin, K. N. Romanyuk, S. V. Makarenko, V. A. Golyashov, A. S. Kozhukhov, I. P. Prosvirin, and Aleksandr Andreevich Shklyaev, Stability of the (0001) surface of the Bi_2Se_3 topological insulator, JETP Lett. **94**, 465 (2011).

[15] Matthew Brahlek, Yong Seung Kim, Namrata Bansal, Eliav Edrey, and Seongshik Oh, Surface versus bulk state in topological insulator Bi_2Se_3 under environmental disorder, Appl. Phys. Lett. **99**, 012109 (2011).

[16] Z. K. Liu, Y. L. Chen, J. G. Analytis, S. K. Mo, D. H. Lu, R. G. Moore, I. R. Fisher, Z. Hussain, and Z. X. Shen, Robust topological surface state against direct surface contamination, Physica (Amsterdam) **44E**, 891 (2012).

[17] R. Valdés Aguilar, A. V. Stier, W. Liu, L. S. Bilbro, D. K. George, N. Bansal, L. Wu, J. Cerne, A. G. Markelz, S. Oh, and N. P. Armitage, Terahertz Response and Colossal Kerr Rotation from the Surface States of the Topological Insulator Bi_2Se_3, Phys. Rev. Lett. **108**, 087403 (2012).

[18] D. J. Kim, S. Thomas, T. Grant, J. Botimer, Z. Fisk, and Jing Xia, Surface Hall effect and nonlocal transport in SmB_6: Evidence for surface conduction, Sci. Rep. **3**, 3150 (2013).

[19] Murong Lang, Liang He, Faxian Xiu, Xinxin Yu, Jianshi Tang, Yong Wang, Xufeng Kou, Wanjun Jiang, Alexei V. Fedorov, and Kang L. Wang, Revelation of topological surface states in Bi_2Se_3 thin films by *in situ* Al passivation, ACS Nano **6**, 295 (2012).

[20] H. D. Li, Z. Y. Wang, X. Kan, X. Guo, H. T. He, Z. Wang, J. N. Wang, T. L. Wong, N. Wang, and M. H. Xie, The van der Waals epitaxy of Bi_2Se_3 on the vicinal Si (111) surface: An approach for preparing high-quality thin films of a topological insulator, New J. Phys. **12**, 103038 (2010).

[21] M. M. Vazifeh and M. Franz, Spin response of electrons on the surface of a topological insulator, Phys. Rev. B **86**, 045451 (2012).

[22] W. A. MacFarlane, C. B. L. Tschense, T. Buck, K. H. Chow, D. L. Cortie, A. N. Hariwal, R. F. Kiefl, D. Koumoulis, C. D. P. Levy, I. McKenzie, F. H. McGee, G. D. Morris, M. R. Pearson, Q. Song, D. Wang, Y. S. Hor, and R. J. Cava, β-detected NMR of $^8Li^+$ in Bi, Sb, and the topological insulator $Bi_{0.9}Sb_{0.1}$, Phys. Rev. B **90**, 214422 (2014).

[23] P. A. Sharma, A. L. Lima Sharma, M. Hekmaty, K. Hattar, V. Stavila, R. Goeke, K. Erickson, D. L. Medlin, M. Brahlek, N. Koirala *et al.*, Ion beam modification of topological insulator bismuth selenide, Appl. Phys. Lett. **105**, 242106 (2014).

[24] N. Wakeham, Y. Q. Wang, Z. Fisk, F. Ronning, and J. D. Thompson, Surface state reconstruction in ion-damaged SmB_6, Phys. Rev. B **91**, 085107 (2015).

[25] C. W. Groth, M. Wimmer, A. R. Akhmerov, J. Tworzydło, and C. W. J. Beenakker, Theory of the Topological Anderson Insulator, Phys. Rev. Lett. **103**, 196805 (2009).

[26] Dongwei Xu, Junjie Qi, Jie Liu, Vincent Sacksteder, X. C. Xie, and Hua Jiang, Phase structure of the topological Anderson insulator, Phys. Rev. B **85**, 195140 (2012).

[27] Zohar Ringel, Yaacov E. Kraus, and Ady Stern, Strong side of weak topological insulators, Phys. Rev. B **86**, 045102 (2012).

[28] Gerald Schubert, Holger Fehske, Lars Fritz, and Matthias Vojta, Fate of topological-insulator surface states under strong disorder, Phys. Rev. B **85**, 201105 (2012).

[29] Quansheng Wu, Liang Du, and Vincent E. Sacksteder, Robust topological insulator conduction under strong boundary disorder, Phys. Rev. B **88**, 045429 (2013).

[30] Quansheng Wu and Vincent E. Sacksteder, Bulk effects on topological conduction in three-dimensional topological insulators, Phys. Rev. B **90**, 045408 (2014).

[31] Tudor D. Stanescu, Victor Galitski, and S. Das Sarma, Topological states in two-dimensional optical lattices, Phys. Rev. A **82**, 013608 (2010).

[32] Michael Buchhold, Daniel Cocks, and Walter Hofstetter, Effects of smooth boundaries on topological edge modes in optical lattices, Phys. Rev. A **85**, 063614 (2012).

[33] A. H. Castro Neto, F. Guinea, N. M. R. Peres, K. S. Novoselov, and A. K. Geim, The electronic properties of graphene, Rev. Mod. Phys. **81**, 109 (2009).

[34] H.-M. Guo, G. Rosenberg, G. Refael, and M. Franz, Topological Anderson Insulator in Three Dimensions, Phys. Rev. Lett. **105**, 216601 (2010).

[35] Liang Chen, Qin Liu, Xulin Lin, Xiaogang Zhang, and Xunya Jiang, Disorder dependence of helical edge states in HgTe/CdTe quantum wells, New J. Phys. **14**, 043028 (2012).

[36] Koji Kobayashi, Tomi Ohtsuki, and Ken-Ichiro Imura, Disordered Weak and Strong Topological Insulators, Phys. Rev. Lett. **110**, 236803 (2013).

[37] Shi-Ting Lee, Shin-Ming Huang, and Chung-Yu Mou, Stability of Z_2 topological order in the presence of vacancy-induced impurity band, J. Phys. Condens. Matter **26**, 255502 (2014).

[38] Chao-Xing Liu, Xiao-Liang Qi, HaiJun Zhang, Xi Dai, Zhong Fang, and Shou-Cheng Zhang, Model Hamiltonian for topological insulators, Phys. Rev. B **82**, 045122 (2010).

[39] Shinsei Ryu and Kentaro Nomura, Disorder-induced quantum phase transitions in three-dimensional topological insulators and superconductors, Phys. Rev. B **85**, 155138 (2012).

[40] Koji Kobayashi, Tomi Ohtsuki, Ken-Ichiro Imura, and Igor F. Herbut, Density of States Scaling at the Semimetal to Metal Transition in Three Dimensional Topological Insulators, Phys. Rev. Lett. **112**, 016402 (2014).

[41] Björn Sbierski, Gregor Pohl, Emil J. Bergholtz, and Piet W. Brouwer, Quantum Transport of Disordered Weyl Semimetals at the Nodal Point, Phys. Rev. Lett. **113**, 026602 (2014).

[42] Alexander Weiße, Gerhard Wellein, Andreas Alvermann, and Holger Fehske, The kernel polynomial method, Rev. Mod. Phys. **78**, 275 (2006).

[43] J. B. Pendry, A. MacKinnon, and P. J. Roberts, Universality classes and fluctuations in disordered systems, Proc. R. Soc. A **437**, 67 (1992).

[44] Keith Slevin, Peter Markoš, and Tomi Ohtsuki, Reconciling Conductance Fluctuations and the Scaling Theory of Localization, Phys. Rev. Lett. **86**, 3594 (2001).

[45] Bernhard Kramer, Tomi Ohtsuki, and Stefan Kettemann, Random network models and quantum phase transitions in two dimensions, Phys. Rep. **417**, 211 (2005).

[46] Wei Zhang, Rui Yu, Hai-Jun Zhang, Xi Dai, and Zhong Fang, First-principles studies of the three-dimensional strong topological insulators Bi_2Te_3, Bi_2Se_3 and Sb_2Te_3, New J. Phys. **12**, 065013 (2010).

[47] D. O. Scanlon, P. D. C. King, R. P. Singh, Alberto De La Torre, S. McKeown Walker, G. Balakrishnan, Félix Baumberger, and C. R. A. Catlow, Controlling bulk conductivity in topological insulators: Key role of anti-site defects, Adv. Mater. **24**, 2154 (2012).

[48] R. J. Cava, Huiwen Ji, M. K. Fuccillo, Q. D. Gibson, and Y. S. Hor, Crystal structure and chemistry of topological insulators, J. Mater. Chem. C **1**, 3176 (2013).

[49] J. W. McIver, D. Hsieh, H. Steinberg, P. Jarillo-Herrero, and N. Gedik, Control over topological insulator photocurrents with light polarization, Nat. Nanotechnol. **7**, 96 (2012).

[50] Jean K. Platten, The Soret effect: A review of recent experimental results, J. Appl. Mech. **73**, 5 (2006).

[51] Yong-Jung Kim, Einstein's random walk and thermal diffusion, arXiv:1307.4460.

[52] M. A. Rahman and M. Z. Saghir, Thermodiffusion or Soret effect: Historical review, Int. J. Heat Mass Transfer **73**, 693 (2014).